

VELOCITY DIFFERENCE OF IONS AND NEUTRALS IN SOLAR PROMINENCES

E. WIEHR¹, G. STELLMACHER², H. BALTHASAR³, AND M. BIANDA⁴

Draft version August 31, 2021

ABSTRACT

Marked velocity excesses of ions relative to neutrals are obtained from two time series of the neighboring emission lines He I 5015 Å and Fe II 5018 Å in a quiescent prominence. Their Doppler shifts show time variations of quasi-periodic character where the ions are faster than the neutrals $1.0 \leq V_{macro}(\text{Fe II})/V_{macro}(\text{He I}) \leq 1.35$ in series-A and, respectively, ≤ 1.25 in series-B. This 'ratio excess' confirms our earlier findings of a 1.22 ion velocity excess, but the present study shows a restriction in space and time of typically 5 Mm and 5 min.

The ratio excess is superposed by a time and velocity independent 'difference excess' $-0.3 \leq V_{macro}(\text{Fe II}) - V_{macro}(\text{He I}) \leq +0.7 \text{ km s}^{-1}$ in series-A (also indicated in series-B). The high repetition rate of 3.9 sec enables the detection of high frequency oscillations with several damped 22 sec periods in series-A. These show a ratio excess with a maximum of 1.7. We confirm the absence of a significant phase delay of He neutrals with respect to the Fe ions.

Subject headings: techniques: spectroscopic - methods: observational - Sun: prominences

1. INTRODUCTION

Charged particles may be faster than neutrals in a partially ionized and weakly collisional magnetized plasma (cf. review by Ballester et al., 2018). This ion drift can be described by a multi-fluid model, where the different species interact by weak coupling processes (Gilbert et al. 2002). For a detailed study of this effect, quiescent solar prominences offer a particularly good example, since they allow higher resolution in space and time than stellar objects. The observed emission of lines from neutrals, as He I, shows that the prominence plasma is not fully ionized.

A velocity excess of ions over neutrals in prominences was observed and discussed in recent papers. Whereas Khomenko et al. (2016) found such an excess in restricted prominence areas with high velocities of short-lived transients, Wiehr et al. (2019) found systematically larger ion shifts through an evolutionary stable prominence. Besides larger Doppler shifts, prominence emissions also show broader line widths for ions than for neutrals (Ramelli et al., 2012, Fig.5; Stellmacher and Wiehr, 2015, Fig.1). This suggests an excess of non-thermal broadening by higher ion velocities on a very small scale.

Here, we study the excess of macro velocity of ions over neutrals in time and space from high resolution time series. We extend and improve former observations of the alternately measured Na I 5896 Å (D₁) and Sr II 4078 Å lines by simultaneous observations of the neighboring lines He I 5015.7 Å (singlet) and Fe II 5018.4 Å. Their small wavelength distance of 2.7 Å avoids influences by the refraction in Earth's atmosphere, which are a relevant problem for time-series observations, since the direction of refraction rotates with respect to the solar disk coordinates (cf. Wiehr et al., 2019).

Parasitic light, superposing the prominence emission with an absorption spectrum, shows different rotational Doppler shift than the prominence emission lines (cf. Wiehr et al.,

2019). This may introduce problems if a reference spectrum for the parasitic light cannot be taken in the immediate neighborhood, as for laterally extended prominences.

2. OBSERVATIONS

We observed a laterally small prominence at the east limb, 5° North on June 28, 2019, from 7:45 UT through 8:25 UT (Fig.1) with the 45 cm aperture Gregory-Coudé telescope and its Czerny Turner spectrograph (f=10 m) of the swiss observatory Istituto Ricerche Solari Locarno. A fixed slit of correspondingly 1.5 arcsec width (1000 km on the Sun) was oriented perpendicular to the solar limb.

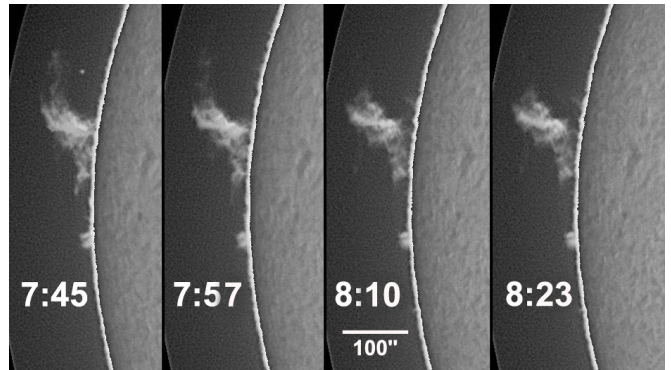


FIG. 1.— $H\alpha$ image sequence of the prominence at the east limb, 5° north from June 28, 2019, (Leamouth observatory); north direction is upwards; the 100'' bar corresponds to 73.4 Mm.

We took time series of the emission lines He I 5015.7 Å and Fe II 5018.4 Å. Their brightness allowed a repetition rate of 3.9 sec, which is 11 times faster than that of Wiehr et al. (2019), the spatial resolution being almost the same. Series-A with 105 spectra (7:45-7:52 UT) shows smooth emissions of He and Fe II along the slit (upper part of Fig. 2). Series-B with 460 spectra (7:55-8:25 UT) shows brighter emissions with marked Doppler shifts and evolutionary time variations (well visible in the lower part of Fig. 2). Sufficiently bright emissions of the faint lines occur in height levels of 31 Mm - 50 Mm above the solar limb, the 31 Mm boundary marking the lower edge of the prominence main body seen in $H\alpha$

ewiehr@gwdg.de, hbalthasar@aip.de, mbianda@irsol.ch

¹ Institut für Astrophysik, D-37077 Göttingen, Germany

² Institut d'Astrophysique, F-75014 Paris, France

³ Leibniz-Institut für Astrophysik, D-14482 Potsdam, Germany

⁴ Istituto Ricerche Solari Locarno, Università della Svizzera italiana, CH-6605 Locarno, Switzerland

(cf. Fig. 1). Beyond spectrum 320 of series-B (7:57 UT) this edge started to uplift with $\approx 9 \text{ km s}^{-1}$ (dashes in Fig.2), and the spectra show increasingly fragmented emissions with line satellites, announcing the sudden disappearance at 9:45 UT.

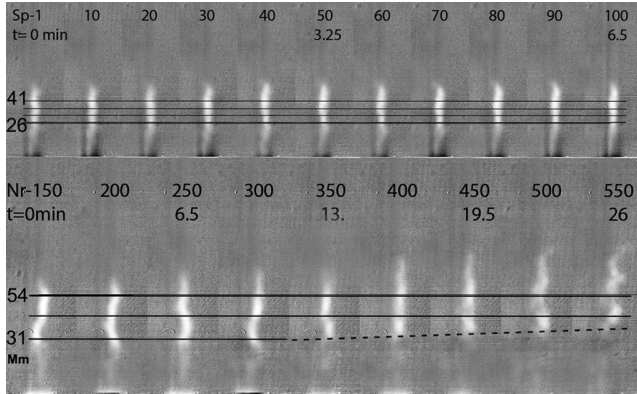


FIG. 2.— Time sequence of the Fe II 5018.4 Å emission spectra in prominence E5N for series-A (upper) and B (lower image part). Scan rows at different height above the limb are marked by full lines; for series-B the lower emission boundary lifts up with $\approx 9 \text{ km s}^{-1}$ (dashed line) after 13 min of observation (spectra with no. ≤ 320); the spatially fragmented emissions in the last two spectra (500 and 550; recorded at 8:18 and 8:21) announce the sudden disappearance at 9:45 UT.

3. DATA REDUCTION

In order to remove parasitic light superposing the emission lines we use spectra of the 'aureola' taken immediately before and after the prominence time series at a slit position in the immediate prominence neighborhood. (For details of the reduction procedure see Ramelli et al., 2012). We average 9 CCD rows, each 257 km wide (0.35 arcsec), to adapt the effective spatial resolution to the slit width.

As wavelength reference for Doppler shifts we determine the centers of the absorption lines Ti I 5016.1, Fe I 5016.9 and Ni I 5017.5, before removing the superposed parasitic light in each individual spectrum, fitting polynomials of second degree. This wavelength reference from the aureole is independent of complex photospheric velocity fields (e.g. oscillations and granular blue shift), which interfere if disk center spectra are used for a wavelength calibration.

We correct the velocities of each individual spectrum for the shift of the three absorption lines relative to their position in the aureola spectra. The resulting macro-velocities are thus free from spectrograph drifts and from slow terms of spectrograph seeing. The two slit positions chosen for the emission spectra and for the aureola spectra aside the prominence, have slightly different inclinations to the solar limb. Hence, their absorption lines show slightly different variation of rotational Doppler shifts along the slit. However, this effect is negligible since the prominence is small and the two slit positions are thus rather close.

The wavelength reference is taken at heights between 40'' and 75'' above the limb, where the aureole spectrum is 1.4 km s^{-1} less blue-shifted than the rotational shift of the east limb (for details see Wiehr et al., 2019). We correspondingly correct the deduced Doppler shifts, thus referring to a co-rotating reference system relative to the photosphere below the prominence.

For the determination of macro-shifts and full widths at half maximum we fit single Gaussians to the upper part of

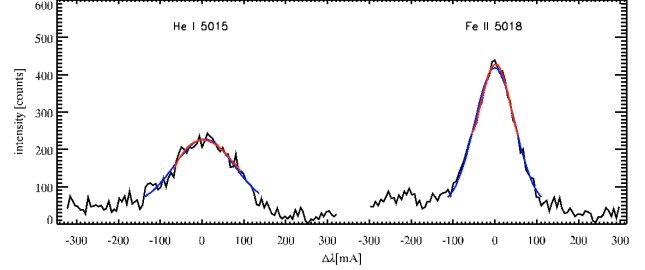


FIG. 3.— Example of the finally obtained emission profiles of He I 5015.7 Å and Fe II 5018.4 Å. Blue curves give the Gaussian, red curves the polynomial fit.

the emission profile. Alternately, we fit polynomials of fourth degree, which better represent asymmetric line profiles. The macro velocities obtained by both methods differ by less than 1%, indicating that the observed profiles of both emission lines are indeed largely symmetric. We therefore use the Gaussian fits, which give an estimated accuracy of $\approx 20 \text{ m/s}$ for the macro velocities

Fig 3 shows an example of finally obtained emission profiles. That of Fe II is narrower due to the 14 times higher mass of Fe. The noise is low enough to ensure reasonable fits.

4. RESULTS

4.1. Time series-B

Doppler-time sequences of Fe II 5018.4 (full lines) and He I 5015.7 (dashed lines) are shown in Fig. 4 for a 4-spectra mean (15.6 s resolution) of the first 17 min of series-B. The macro shifts give quasi-periodic velocity variations of several km s^{-1} with almost equal amplitudes for both lines. They are superposed by a velocity difference of Fe II relative to He I. This 'difference excess' is nearly constant with time (i.e. spectrum number), independent on the velocity itself and diminishes at larger heights.

If we remove the time-constant ion drift, most of the differences between the Fe II and the He I velocities disappear (Fig. 5), reflecting the largely equal amplitudes. However in the time interval of minute 4.5 through 9.5 of series-B a superposed excess of Fe II velocities becomes visible at heights $\leq 40 \text{ Mm}$ above the limb. In contrast to the 'difference excess', this excess is related to the velocity itself and thus a 'ratio excess'. Scatterplots (e.g. Fig. 6) show that it smoothly varies with height between $32 < h < 37 \text{ Mm}$ and disappears for $h > 40 \text{ Mm}$. Its maximum amounts to $V_{\text{macro}}(\text{Fe II})/V_{\text{macro}}(\text{He I})=1.25$, in agreement with Wiehr et al. (2019).

In Fig. 7 we show the time variation of the difference of Fe II and He I velocities. [Note that the ordinate scale is about five times expanded as compared to Figs. 4 and 5.] The nearly constant values through the first 4.5 min again reflect the largely equal velocity amplitudes of Fe II and He I. We mark the shifts applied to transform Fig. 4 into Fig. 5 by dashed lines and vertical arrows. These vary from -0.35 km s^{-1} ('blue excess') at $h=30.8 \text{ Mm}$ to $+0.6 \text{ km s}^{-1}$ ('red excess') at $h=39.8 \text{ Mm}$ above the limb, yielding an almost perfectly linear gradient of 1 km s^{-1} over 11.6 Mm.

The onset of the Fe II ratio excess at spectrum-70 agrees with that in Fig. 5. We thus find two species of ion drifts: (i) a velocity difference excess largely independent of the velocity itself (even through the marked velocity increase between spectrum-40 and -70); and (ii) a ratio excess depending on

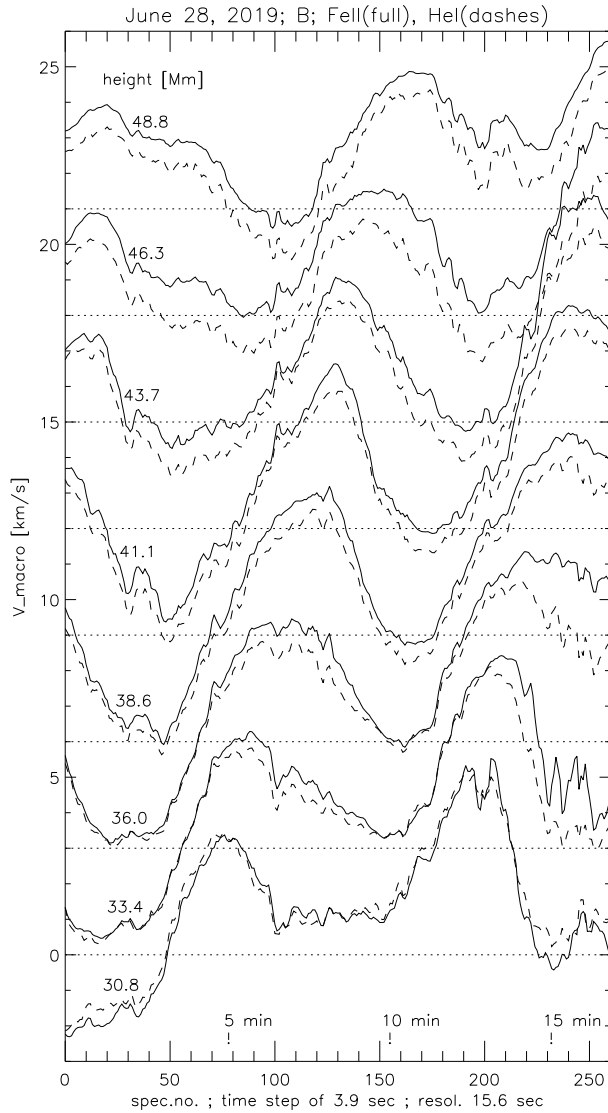


FIG. 4.— Macro velocities of Fe II 5018.4 Å (full) and He I 5015.7 Å (dashed) relative to the photosphere below the prominence for series-B; each scan averages over 9 CCD rows (i.e. 2.3 Mm resolution); time scale integrated over 4 spectra, (15.6 s time resolution); scans shifted to each other by 3 km s^{-1} (dotted lines); height levels are indicated.

velocity, and restricted in space and time.

Beyond spectrum-210 (> 13.5 min of recording series-B) the macro velocity of the He emission line stays increasingly behind that of the Fe ions (cf. Fig. 4). The corresponding spectra show marked fragmentation (cf. Fig. 2) and motions along the slit direction. Differences between Gaussian and poly fits indicate asymmetric profiles caused by superposition of line satellites. This indicates the onset of evolutionary velocity changes announcing the sudden disappearance. We thus restrict our data analysis of series-B to the first 210 spectra.

4.2. Time series-A

The spectra of series-A are characterized by rather narrow and symmetric emission lines (cf. Fig. 2). Doppler-time sequences show quasi-periodic velocity perturbations with amplitudes increasing with height from 0.35 to 1.45 km s^{-1} over the range $30 - 44$ Mm (Fig 8). Above 40 Mm we find a velocity excess $1.0 \leq V_{\text{macro}}(\text{Fe II})/V_{\text{macro}}(\text{He I}) \leq 1.35$. At lower heights ($h \leq 39$ Mm) no ratio excess is observed, however, a

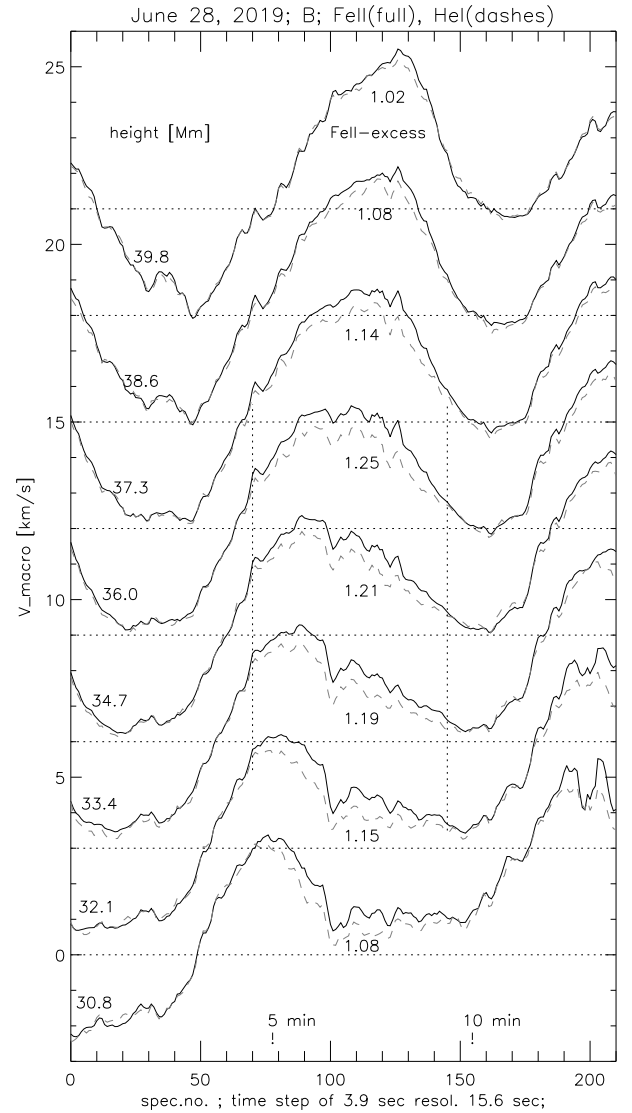


FIG. 5.— Same as Fig.4, but the He I velocity (dashes) shifted to fit that of Fe II over a smaller height range in the first 70 spectra of series-B; the scan rows are vertically displaced by $+3 \text{ km s}^{-1}$; dotted vertical lines mark the limits of time and space regimes with excess velocity ratio > 1.1 ; height levels are indicated.

general shift ('difference excess') is indicated in the lowest three scan rows at $h \leq 36$ Mm (cf. Fig 8).

4.3. High frequency perturbations

The high repetition rate of 3.9 s enables the detection of short-period velocity variations visible in the middle scan rows of spectra 40-90 in Fig. 8. To make them visible, we suppress the long-term velocity perturbations, by subtracting the 10-spectra means from the 2-spectra means seen in Fig. 8. The resulting time series in Fig. 9 shows at the height level 39.8 Mm an almost perfect oscillation with decreasing amplitude through interval minute 2.6 to 5.5 (spectra 40-90).

The power spectrum Fig. 10 of the corresponding height range $38 < h < 41$ Mm over the total series-A of 105 spectra shows a pronounced peak at 46 mHz (22 sec) with a significance of 99.9% for Fe II and 99.0% for He I (for details see Balthasar, 2003). Since the power maxima represent the square of the velocity amplitudes, we obtain from the square roots of the power maxima of the two emission lines their am-

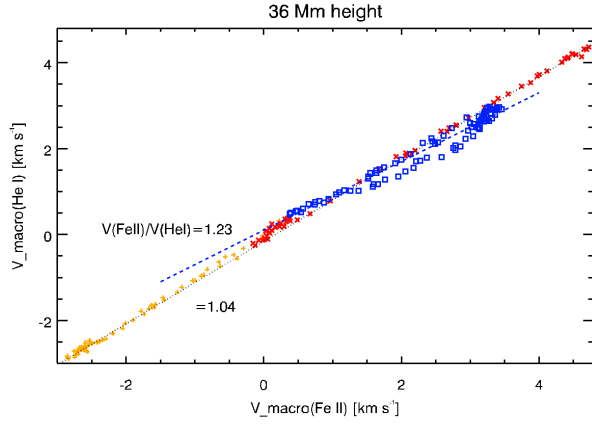


FIG. 6.— Scatterplot of He I 5015.7 and Fe II 5018.4 velocities of series-B at the height $h = 36 \pm 1$ Mm with maximum ion velocity excess; spectra-0-69 (yellow +) and 151-210 (red X) give no excess; spectra-70-150 (blue □) give an excess of 1.23.

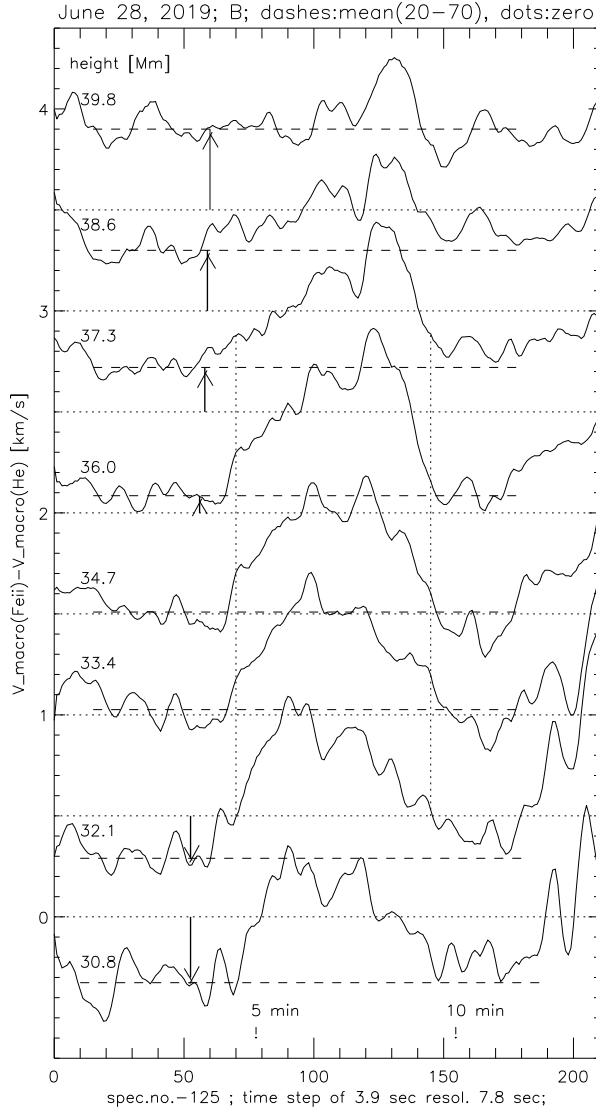


FIG. 7.— Time variation of the velocity difference Fe II - He I, used to transform Fig.3 to Fig.4: horizontal dashed lines mark the offset taken from spectra-0 to 69; vertical arrows visualize the respective blue and red shifts.

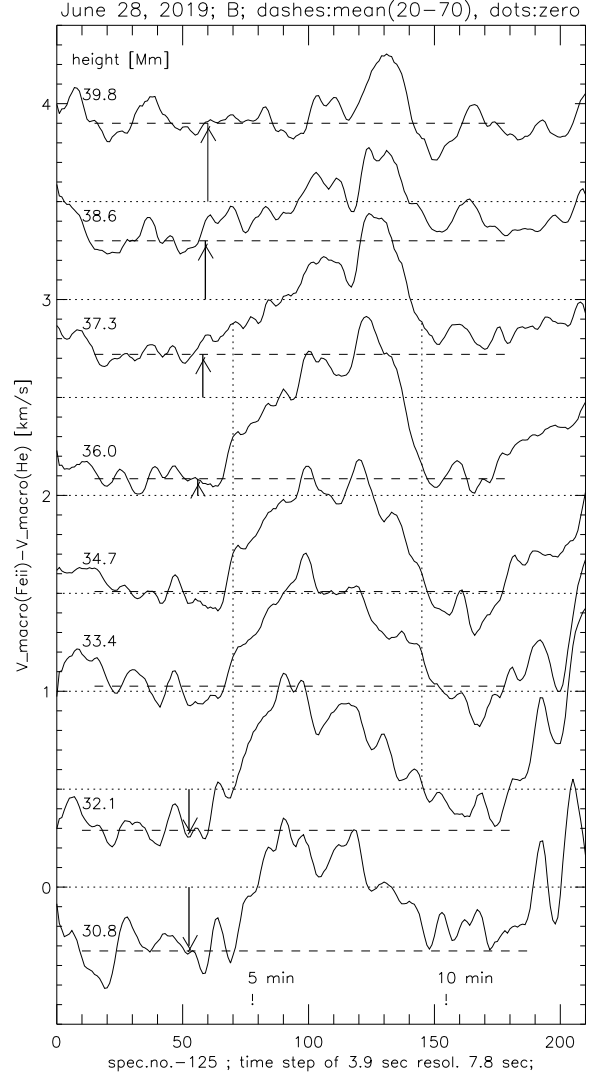


FIG. 8.— Velocity variation of He I (dashed) and Fe II (full line) in series-A; each scan averaged over 9 rows (2.3 Mm resolution); time scale integrated over 2 spectra (7.8 s resolution) in the height range 30.8-46.3 Mm; the scans are shifted towards each other by 1.0 km s^{-1} .

plitude ratio. The velocity excess in the interval of 22 sec oscillation amounts to 1.7. In the subinterval with pronounced oscillations (spectra 40-90) scatterplots of the He I and Fe II velocities show that the velocity excess has a spatial variation almost parallel to that of the large time-scale ratio of series-A (cf. section-4.2).

In series-B we also find high frequency variations with periods near 25 s in restricted intervals of space and time. These, however, show only few cycles and give thus no significant peak in the power spectra. For the high frequency oscillations we do not find a significant phase shift between Fe II and He I.

5. DISCUSSION

The observation of this prominence started ≈ 100 min before its sudden disappearance. It shows two species of ion excess: (i) a velocity difference $V_{macro}(\text{Fe II}) - V_{macro}(\text{He I})$ and (ii) a velocity ratio $V_{macro}(\text{Fe II})/V_{macro}(\text{He I})$. The marked 'difference excess' found in series-B increases linearly with height from -0.3 km s^{-1} (blue shift) at 30.9 Mm height to $+0.7 \text{ km s}^{-1}$ (red shift) at 42.6 Mm height (left panel of Fig. 11). A similar effect was found in Wiehr et al. (2019)

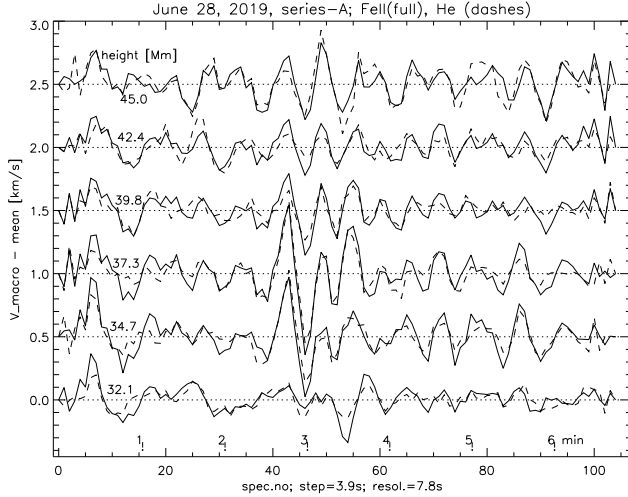


FIG. 9.— Difference of macro shifts from 2 and 10 spectra means (7.8s and 39s time resolution) for the height range $30.8 \leq h \leq 43.7$ Mm, covering the 22 s oscillation region.

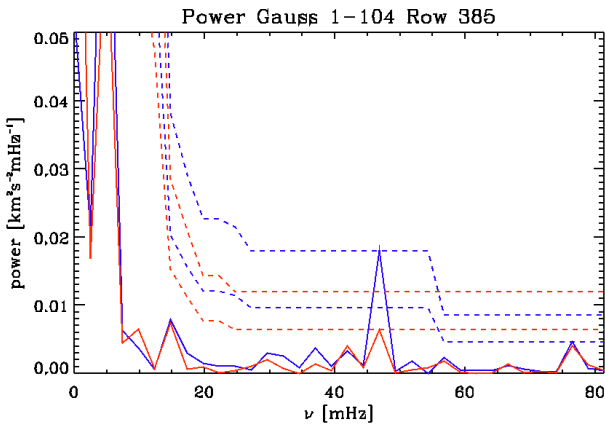


FIG. 10.— Power spectrum of Fe II (blue) and He I (red) at $h=40$ Mm of series-A, showing a pronounced peak at 46 mHz (22 sec period); the 99% and 99.9% significance levels are indicated (dashed); the square root of the power maxima ratio of both emission lines gives a velocity excess of 1.7.

where such difference excess increased between 3.3 and 39 Mm from $+0.4$ to $+2.1$ km s^{-1} . [Note that the velocities refer in both papers to the photosphere below the prominence.]

If we remove the time constant difference excess, we find in the interval minutes 4.5 through 9.5 of series-B a superposed ratio excess that varies smoothly between 31 and 38 Mm with a flat maximum of $V_{\text{macro}}(\text{Fe II})/V_{\text{macro}}(\text{He I}) \approx 1.25$ (yellow line in Fig. 11). In series-A we find a ratio excess with a maximum of 1.35 (full green line in Fig. 11). Both excess values are close to that of 1.22 in Wiehr et al. (2019).

In those data the ratio excess was observed along the complete slit length. The present data, however, show a spatial restriction of the ratio excess to 3 - 8 Mm height. Since our observations were performed at a single cut through the prominence from a fixed slit position, we have no information about the two-dimensional spatial distribution of the ion velocity excess. In both studies we do not find phase shifts between the Fe II and He I velocities, in agreement with Khomenko et al. (2016) and Wiehr et al. (2019).

The pronounced high frequency oscillations with 22 s period show an ion velocity excess with a maximum of 1.7 in a spatial interval of about 3 Mm. These short periods occur

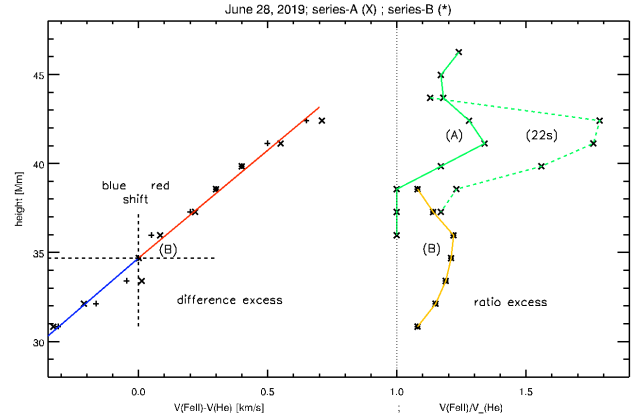


FIG. 11.— Dependence of the difference excess (left) and the ratio excess (right side) on height above the solar limb for series-B (yellow line), series-A and its 22 s oscillation (green lines); difference excess determined visually (+) and by subtraction (X); its transition between blue- and red-shift occurs at 34.5 Mm height above the limb (dash-line cross).

only in the time interval of minute 3 through 6 in series-A (cf. Fig. 9). They do not vary with height, indicating stationary waves. Balthasar et al. (1993) find 30 sec periods in a quiescent prominence, and Locans et al. (1983) observe 43 sec periods in a coronal arch system around a prominence. In contrast to these high-frequency oscillations with several pronounced periods of decreasing amplitude (i.e. damped cf. Fig. 9), do the quasi-periodic velocity perturbations of longer time scale (cf. Figs. 4 and 8) show only few extrema with nearly amplitude. This quasi-periodic character is typical for most velocity time series observations in quiescent prominences (cf. Wiehr, 2004).

The observation of a spatial and temporal restriction of the ion excess indicates an interaction of a structured velocity field with the prominence magnetic field. An impressive view of such complex velocity field in a prominence is seen in the Hinode observations by Berger et al. (2010). The ion velocity excess will occur only under particular conditions of such a chaotic velocity field, in accordance with the findings of Khomenko et al. (2016) of an excess only in short-lived transients with high velocities. These authors argue that the balance between ions and neutrals "is usually lost a locations with large individual velocities or large spatial or temporal gradients", and further that they "are smoothed by interactions on relatively short timescales (typically of the order of minutes)". The here described observations of the ion-neutral velocity ratio excesses are indeed limited in space and time.

The present observations were made ≈ 100 min before the sudden disappearance of the prominence, which may announce itself by the increasingly chaotic velocity field. In contrast, the finding of a systematic excess during the full observing time through the whole prominence time (Wiehr et al., 2019) was obtained from a long-living quiescent prominence. Hence the dynamic behavior of the prominence seems to play an essential role for the detectability of an ion velocity excess over neutrals.

6. REFERENCES

- Ballester, J. L.; Alexejev, I.; Collados, M.; Downes, T.; Pfaff, R. F.; Gilbert, H.; Khodachenko, M.; Khomenko, E.; Shaikhislamov, I. F.; Soler, R.; Vázquez-Semadeni, E.; Zaqarashvili, T.: 2018, *SSRv* 214, 58 (DOI: 10.1007/s11214-018-0485-6)
- Balthasar, H.: 2003, *Sol. Phys.* 218, 85 (DOI: 10.1023/B:SOLA.0000013028.11720.0d)
- Balthasar, H., Wiehr, E., Schleicher, H., Wöhl, H.: 1993, *A&A* 277, 635
- Berger, T. E., Slater, G., Hurlburt, N. Shine, R., Tarbel, T., Title, A., Lites, B. W., Okamoto, T. J., Ichimoto, K., Katsukawa, Y., Magara, T., Suematsu, Y., Shimizu, T.: 2010, *ApJ* 716, 1288 (DOI: 10.1088/0004-637X/716/2/1288)
- Gilbert, H. R., Hansteen, V. H., Holzer, T. E.: 2002, *ApJ* 577, 464 (DOI: 10.1086/342165)
- Khomenko, E., Collados, M., Diaz, A.J.: 2016, *ApJ* 823, 132 (DOI: 10.3847/0004-637X/823/2/132)
- Locans, V., Zhugzda, D., Koutchmy, S.: 1983, *A&A* 120, 185
- Ramelli, R., Stellmacher, G., Wiehr, E., Bianda, M.: 2012, *Sol. Phys.* 281, 697 (DOI: 10.1007/s11207-012-0118-2)
- Stellmacher, G., Wiehr, E.: 2015, *A&A* 581, 141 (DOI: 10.1051/0004-6361/201322781)
- Wiehr, E.: 2004, Proceedings of 'SOHO 13 - Waves, Oscillations and Small-Scale Transient Events in the Solar Atmosphere: A Joint View from SOHO and TRACE'. 29 September - 3 October 2003, Palma de Mallorca, Balearic Islands, Spain (ESA SP-547, January 2004).
- Wiehr, E., Stellmacher, G., Bianda, M.: 2019, *ApJ* 873, 125 (DOI: 10.3847/1538-4357/ab04a4)